Journal of Sound and Vibration (2000) **229**(4), 859–878
doi:10.1006/jsvi.1999.2524, available online at http://www.idealibrary.com on IDEAL®

PREDICTION OF LOW-FREQUENCY TONES PRODUCED BY FLOW THROUGH A DUCT WITH A GAP

S. M. GRACE

Aerospace and Mechanical Engineering Department, Boston University,
110 *Cummington St., Boston, MA* 02215, *U.S.A.*

(*Received* 2 *September* 1998, *and in final form* 9 *July* 1999)

A method is presented for predicting the frequencies of tones produced by high Reynolds number, subsonic flow through a duct with a gap. An inviscid, linear model of the fluid motion is developed in which the shear layer delimiting the jet formed between the inlet and exit of the duct gap is modelled as a vortex sheet. The linear analysis is used to calculate the Rayleigh conductivity parameter which is then analyzed to find the frequency dependence of the shear layer behavior. The calculations for the case when an external load is applied across the shear layer have been carried out for Strouhal numbers from 0 to 10, Mach numbers from 0·001 to 0·5, and a gap length-to-diameter ratio of 0·5 to 2·0. The resonant frequencies have been calculated for Mach numbers ranging from 0·001 to 0·8 at a length-to-diameter ratio of 1·0. The results for the forced motion in the low Mach number limit compare well with previous incompressible predictions for flow past wall apertures. The resonant frequency predictions have been validated at the Mach number of 0·52 through comparison with experimental data.

1. INTRODUCTION

Flow through a thin-walled duct with a gap can produce tonal low-frequency noise. An example of this phenomenon was reported by Paterson *et al.* [1]. Their paper describes the development of an anechoic facility which includes an open-jet wind tunnel. In their experiments, the tunnel itself created broadband noise as well as tones. They attributed the tones to "edge tone interaction between the contraction outlet and the jet collector". The example illustrates tones created in the absence of an external force. The frequency of such tones will be referred to as *resonant* frequencies throughout this paper. In addition to resonant frequencies, other tones may be created by flow through a duct with a gap when there exists an external time-dependent load on the system. The frequency of these tones will be referred to as the *forced* frequencies.

When the flow Reynolds number is high, both the resonant and forced frequencies of a duct/gap configuration can be predicted using a linearized model of the fluid dynamics. For high Reynolds number, the shear layer that forms downstream of the sharp edge due to viscous forces can be inviscidly approximated

0022-460X/00/040859 + 20 $35.00/0

as a vortex sheet, and vortex shedding from a wall edge can be simulated by imposing the Kutta condition.

In this research, a linearized model with imposed Kutta condition and embedded vortex sheet approximation is used to calculate the forced and resonant frequencies of flow through a *cylindrical* duct with gap as shown in Figure 1. The method hinges upon analyzing a frequency-dependent parameter known as the Rayleigh conductivity $K_R(\omega)$ which is defined as

$$\rho_\infty \frac{\partial Q(t)}{\partial t} = -\frac{1}{2\pi}\int_{-\infty}^{\infty} K_R(\omega)\, p_i(\omega)\, \mathrm{e}^{-\mathrm{i}\omega t}\, \mathrm{d}\omega, \tag{1}$$

where $Q(t)$ is the volume flux through the outer edge of the duct which contains the shear layer, and $p_i(\omega)$ is a Fourier component of an applied load. The applied load p_i is assumed to be spatially constant along the shear layer in the opening for this calculation. This assumption is consistent with focusing one's attention on the response of the shear layer to long-wavelength disturbances.

The net volume flux through the boundaries of the duct opening is proportional to the total displacement of the vortex sheet in the normal direction to the sheet, so that

$$Q = \int v_r\, \mathrm{d}A = \int_{-\infty}^{\infty} \frac{\mathrm{D}\zeta_r}{\mathrm{D}t}\, \mathrm{d}A, \tag{2}$$

where v_r is the radial velocity, ζ_r is the normal displacement, $(\mathrm{D}/\mathrm{D}t) = (\partial/\partial t) + U(\partial/\partial z)$ is the convective derivative, and A is equivalent to the surface area of the curved sides of a cylinder that would fit in the duct opening.

When the applied load p_i is periodic in time with frequency ω, equation (1) can be written as

$$K_R(\omega) = \frac{\mathrm{i}\omega\rho_\infty Q(\omega)}{p_i(\omega)}, \tag{3}$$

where $Q(\omega)$ is the Fourier transform of the volume flux. In a real fluid, $K_R(\omega)$ is generally a complex function of the frequency ω. It was shown in reference [2] that at frequencies ω for which $\mathrm{Im}(K_R(\omega))$ is greater than zero, the shear layer motion will amplify at the expense of the energy in the mean flow. It is at these frequencies then that the configuration can be *forced* to produce a tone. By examination of equation (1) one can see that the resonant frequencies of the system, i.e., the frequencies at which the volume flux will grow naturally, occur at frequencies which coincide with poles of the Raleigh conductivity parameter. It was shown in reference [2] that tone predictions based on this method agreed well with experiments.

The mathematical formulation of the Raleigh conductivity parameter for the thin-walled cylindrical duct is described in section 2. The formulation follows the methodology used in references [3–5] where the vortex sheet displacement is calculated by solving an integral equation and then used in equation (2) to determine the volume flux. The Rayleigh conductivity has been calculated as a function of the reduced frequency, $\bar{\sigma} = \omega a/U$, where a is the radius of the duct and

U is the mean velocity of the fluid through the duct. The results are reported in section 3. The possible forced tones are recorded for flow Mach numbers varying from 0·001 to 0·5 and for duct gap length-to-diameter ratios of 0·5, 1·0, and 1·5. The resonant tones that are computed using the method described in references [6, 7] are tabulated for a length-to-diameter ratio of 1·0 and for Mach numbers from 0·001 to 0·8. Finally, the predicted resonant frequencies are compared with the tones measured by Paterson *et al.* [1] in their experiment.

2. MATHEMATICAL FORMULATION

The Rayleigh conductivity, equation (3), used to determine the frequency bands corresponding to a forced instability or a natural instability, depends on the volume flux Q through the edges of the duct gap region. The determination of Q for the cylindrical duct configuration is detailed in this section and depends heavily on the construction of an appropriate Green's function. The development of the Rayleigh conductivity equation for this research extends prior applications of the Rayleigh conductivity method [2, 6, 4] to include the effects of compressibility.

An inviscid, linear model of the fluid dynamics leads to a Helmholtz equation for the velocity potential inside and outside the cylinder. Specifically, the linearized continuity and Euler equations are

$$\frac{\mathrm{D}_\infty \rho'}{\mathrm{D}t} + \rho_\infty \nabla \cdot \mathbf{u}' = 0, \quad \text{and} \quad \rho_\infty \frac{\mathrm{D}_\infty \mathbf{u}'}{\mathrm{D}t} = -\nabla p', \tag{4, 5}$$

which can be combined to form a single convective wave equation for the unsteady potential ϕ defined as $\nabla\phi = \mathbf{u}$. The adiabatic relation $p' = \rho' c_\infty^2$ is used where c_∞ is the speed of sound. The resulting convective wave equation with constant coefficients can be transformed into the Helmholtz equation in cylindrical co-ordinates by using the Prandtl–Glauert transformation defined as

$$\tilde{r} = \beta_{i,o} r, \quad \tilde{\theta} = \theta, \quad \tilde{z} = z$$

and the transformation

$$\Phi = \phi \mathrm{e}^{\mathrm{i}\omega t} \mathrm{e}^{\mathrm{i}M_{i,o}K_{i,o}\tilde{z}},$$

where M is the Mach number, $\beta = \sqrt{1 - M^2}$, $K = \omega / c_\infty \beta^2$, and the subscripts i, o represent inside and outside the cylinder respectively. Thus, the Helmholtz equation can be written for the transformed velocity potential Φ as

$$(\tilde{\nabla}^2 + K_{i,o}^2)\Phi = 0. \tag{6}$$

For ducted flow, the fluid outside the cylinder is not moving and therefore $U_o = 0$, $M_o = 0$, and $\beta_o = 1{\cdot}0$ but, $U_i = U$, $M_i = M$, and $\beta_i = \beta$.

Solutions to the outer and inner Helmholtz equations are obtained in terms of the normal derivative of the shear layer motion by introducing a Green's function that satisfies

$$(\tilde{\nabla}^2 + K_{i,o}^2)G = 0 \tag{7}$$

for the physical locations $r \lessgtr a$ and the condition

$$\partial G/\partial \tilde{r} = \delta(z - z_0) \tag{8}$$

on the boundary $r = a$. Because the z variable is not affected by the Prandtl–Glauert transformation the $\tilde{}$ notation has been dropped in reference to z. This Green's function is modelled after the one used for the two-dimensional problem of flow past a slot in reference [8].

A Fourier transform of the Helmholtz equation and the boundary condition in the z direction using

$$\int_{-\infty}^{\infty} (\tilde{\nabla}^2 + K^2) G e^{ikz} \, dz = 0, \tag{9}$$

$$\int_{-\infty}^{\infty} \frac{\partial G}{\partial \tilde{r}} \, e^{ikz} \, dz = \int_{-\infty}^{\infty} \delta(z - z_0) \, e^{ikz} \, dz, \tag{10}$$

results in wavenumber components of the transformed Green's function $\hat{G}$ satisfying

$$\frac{1}{\tilde{r}} \frac{\partial}{\partial \tilde{r}} \left(\tilde{r} \frac{\partial}{\partial \tilde{r}} \right) \hat{G} - (k^2 - K^2) \hat{G} = 0,$$

$$\frac{\partial \hat{G}}{\partial \tilde{r}} (\tilde{r} \to \tilde{a}, k, \tilde{a}, z_0) = e^{ikz_0}.$$

The desired Green's function will act as a transfer function in the *near* field of the source and thus the kth Fourier components inside and outside a cylinder of radius a are

$$\hat{G}_i(\tilde{r}, k, \tilde{a}, z_0) = \frac{I_0(\sqrt{k^2 - K_i^2}\, \tilde{r}) \, e^{ikz_0}}{\sqrt{k^2 - K_i^2}\, I_1(\sqrt{k^2 - K_i^2}\, \tilde{a})}, \quad \tilde{r} < \tilde{a},$$

$$\hat{G}_0(r, k, a, z_0) = \frac{-\mathcal{K}_0(\sqrt{k^2 - K_o^2}\, r) \, e^{ikz_0}}{\sqrt{k^2 - K2^o}\, \mathcal{K}_1(\sqrt{k^2 - K_o^2}\, a)}, \quad r > a$$

where I_v and $\mathcal{K}_v$ are the modified Bessel functions of order v. In order to transform the initial Green's functions back to z space, one must calculate

$$G_i = \frac{1}{2\pi} \int_{-\infty}^{\infty} \frac{I_0(\sqrt{k^2 - K_i^2}\, \tilde{r}) \, e^{ik(z_0 - z)} \, dk}{\sqrt{k^2 - K_i^2}\, I_1(\sqrt{k^2 - K_i^2}\, \tilde{a})}, \tag{11}$$

$$G_o = \frac{1}{2\pi} \int_{-\infty}^{\infty} \frac{-\mathcal{K}_0(\sqrt{k^2 - K_o^2}\, r) \, e^{ik(z_0 - z)} \, dk}{\sqrt{k^2 - K_o^2}\, \mathcal{K}_1(\sqrt{k^2 - K_o^2}\, a)}. \tag{12}$$

We are interested in Green's function for the case of $r \to a$ and z close to z_0. When one considers the near field of z, the integrals (11) and (12) can be simplified (see Appendix A). The asymptotic forms of the inner and outer Green's function are

$$G_{i,o} \sim \pm \frac{1}{\pi} \ln(K_{i,o} |z_0 - z|). \tag{13}$$

Once an appropriate Green's function has been determined, it can be used to find the potential at any point along the duct gap opening due to a distribution of sources along the gap opening. For the inner Green's function this gives

$$\Phi_i(\tilde{a}, z_0) = \int G_i(\tilde{a}, z, \tilde{a}, z_0) \frac{\partial \Phi_i(\tilde{a}, z)}{\partial \tilde{\eta}} \, \mathrm{d}z. \tag{14}$$

From the definition of Φ it can be shown that

$$\frac{\partial \Phi_i(\tilde{a}, z)}{\partial \tilde{\eta}} = -\mathrm{e}^{\mathrm{i}MK_i\tilde{z}} \left(-\mathrm{i}\omega + U_i \frac{\partial}{\partial z} \right) \xi_{r_i}(\tilde{a}, z), \tag{15}$$

where ξ_r is the displacement of the vortex sheet in the radial direction (with no β factor taken out and $\mathrm{e}^{-\mathrm{i}\omega t}$ suppressed).

By substituting these relations into equation (14), integrating by parts, and rearranging, one can show that the perturbation velocity potentials inside and outside the duct become

$$\phi_i(\tilde{a}, z_0) = \frac{\mathrm{e}^{-\mathrm{i}MK_i z_0}}{\beta} \left(-\mathrm{i}\omega - \mathrm{i}MK_i U + U \frac{\partial}{\partial z_0} \right) \int \ln(K_i |z_0 - z|) \xi_{r_i}(\tilde{a}, z) \mathrm{e}^{\mathrm{i}MK_i z} \, \mathrm{d}z, \tag{16}$$

$$\phi_o(a, z_0) = -(\mathrm{i}\omega) \int \ln(K_o |z_0 - z|) \xi_{r_o}(a, z) \, \mathrm{d}z. \tag{17}$$

Across the vortex sheet the pressure must be continuous. Without loss of generality, the applied load can be assumed to be inside the duct. Then, inside the duct, there is pressure associated with both the load p_i and the potential flow disturbance described by equation (16). Outside the cylinder there is only pressure associated with the motion of the vortex sheet as described by equation (17); hence, the boundary condition can be written as

$$\mathrm{i}\omega \phi_o(a, z_0) = \frac{p_i}{\rho_\infty} - \left(-\mathrm{i}\omega + U \frac{\partial}{\partial z_0} \right) \phi_i(\tilde{a}, z_0)$$

or

$$\frac{p_i}{\rho_\infty} = \mathrm{i}\omega \phi_o(a, z_0) + \left(-\mathrm{i}\omega + U \frac{\partial}{\partial z_0} \right) \phi_i(\tilde{a}, z_0). \tag{18}$$

The matching of the inner and outer representations of the pressure occurs at the radial location of the cylinder wall in physical space; therefore, the value of ϕ_i at βa is used an the value of ϕ_o at a is used. At this point in the field, $\xi_{r_i}(\beta a, z) = \xi_{r_o}(a, z)$ and therefore when equations (16) and (17) are substituted into equation (18), the governing equation becomes

$$\frac{p_i}{\rho_\infty} = \omega^2 \int \ln(K_o |z_0 - z|) \xi_{r_o} \, \mathrm{d}z + \frac{\mathrm{e}^{-\mathrm{i}MK_i z_0}}{\beta} \left(-\frac{\mathrm{i}\omega}{\beta^2} + U \frac{\partial}{\partial z_0} \right)^2 \times \int \ln(K_i |z_0 - z|) \xi_{r_o} \mathrm{e}^{\mathrm{i}MK_i z} \, \mathrm{d}z. \tag{19}$$

In order to combine the two integrals on the right-hand side of equation (19) a particular solution to the differential equation

$$\left(U^2\frac{\partial^2}{\partial z_0^2} - 2i\frac{\omega U}{\beta^2}\frac{\partial}{\partial z_0} - \frac{\omega^2}{\beta^4}\right) f(z_0) = -\omega^2\beta e^{iMK_i z_0}\int \ln(K_o|z_0 - z|)\xi_r\,dz \quad (20)$$

must be calculated. When $\sigma = \omega/U$ the particular solution can be written as

$$f(z_0) = -\sigma^2\beta\int \xi_r\left[\frac{e^{iMK_i z_0}}{-\sigma^2}(1 + \ln(K_o|z_0 - z|)) + g(z_0 - z)\,e^{-i\sigma z + i(\sigma/\beta^2)z_0}\left(z - z_0 - \frac{i}{\sigma}\right)\right]dz, \quad (21)$$

where g is a function whose derivative with respect to z_0 is $e^{-i\sigma(z_0 - z)}/[-i\sigma(z_0 - z)]$, i.e.,

$$g(z_0 - z) = \begin{cases} \dfrac{\mathrm{Si}(\sigma(z_0 - z)) + i\mathrm{Ci}(\sigma(z_0 - z))}{\sigma}, & z_0 - z \geqslant 0, \\ \dfrac{\mathrm{Si}(\sigma(z_0 - z)) + i\mathrm{Ci}(\sigma(z - z_0))}{\sigma}, & z_0 - z \leqslant 0, \end{cases}$$

with $\mathrm{Si}(x)$ and $\mathrm{Ci}(x)$, the sine and cosine integral functions, defined as

$$\mathrm{Si}(x) = \int_{-\infty}^{x}\frac{\sin(t)}{t}dt, \quad \mathrm{Ci}(x) = \int_{-\infty}^{x}\frac{\cos(t) - 1}{t}dt. \quad (22)$$

All together then, the differential integral equation can be written as

$$\beta\frac{p_i}{\rho_\infty} = e^{-iMK_i z_0}\left(\frac{\sigma^2}{\beta^4} + \frac{2i\sigma}{\beta^2}\frac{\partial}{\partial z_0} - \frac{\partial^2}{\partial z_0^2}\right)\int \xi_r\,\mathrm{Ker}(z_0, z)\,dz, \quad (23)$$

where the kernel is

$$\mathrm{Ker}(z_0, z) = -\sigma^2\beta\left[\frac{e^{iMK_i z_0}}{-\sigma^2}(1 + \ln(K_o|z_0 - z|)) + g(z_0 - z)\,e^{-i\sigma z + i(\sigma/\beta^2)z_0}\left(z - z_0 - \frac{i}{\sigma}\right)\right] + \ln(K_i|z_0 - z|)e^{iMK_i z}. \quad (24)$$

The differential equation part of the expression can be solved to obtain an integral equation for the displacement of the vortex sheet in the radial direction:

$$\int \xi_r(a, z)\,\mathrm{Ker}(z_0, z)\,dz = \alpha_1 e^{i(\sigma/\beta^2)z_0} + \alpha_2 z_0\,e^{i(\sigma/\beta^2)z_0} + \frac{\beta e^{iMK_i z_0}p_i}{\rho_\infty U^2\sigma^2}, \quad (25)$$

where $\alpha_{1,2}$ are unknown constants of integration and the integration can be restricted to the streamwise length of the gap $2Z$ (as shown in Figure 1) because ξ_r vanishes along the solid walls. If the lengths are non-dimensionalized with respect to the radius of the cylindrical duct a and denoted with an overbar, then the

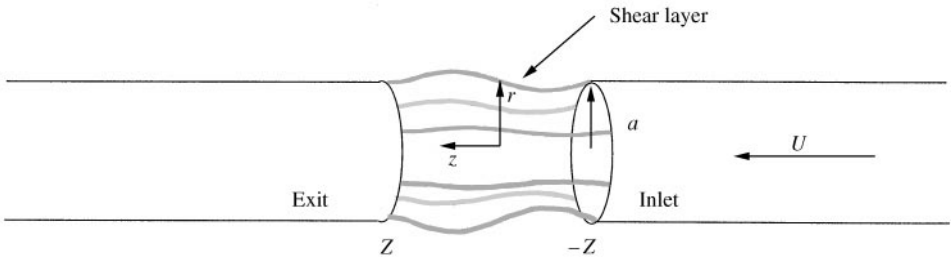

Figure 1. Circular duct with a gap.

reduced frequency becomes

$$\bar{\sigma} = \omega a/U \tag{26}$$

and the limits of integration become $-\bar{Z} = -Z/a$ to $\bar{Z} = Z/a$. For convenience, ξ_r can be non-dimensionalized by

$$\bar{\xi}_r = \frac{\xi_r \rho_\infty U^2 \bar{\sigma}^2}{\beta a p_i}$$

to obtain

$$\int_{-\bar{Z}}^{\bar{Z}} \bar{\xi}_r(\bar{z}) \,\mathrm{Ker}(\bar{z}_0 - \bar{z})\, \mathrm{d}\bar{z} = \bar{\alpha}_1 \mathrm{e}^{\mathrm{i}\bar{\alpha}_1 \bar{z}_0} + \bar{z}_0 \bar{\alpha}_2 \mathrm{e}^{\mathrm{i}\bar{\alpha}_1 \bar{z}_0} + \mathrm{e}^{\mathrm{i}(M^2/\beta^2)\bar{\sigma}\bar{z}_0}. \tag{27}$$

The integral equation is then solved for $\bar{\xi}_r$ and $\bar{\alpha}_{1,2}$. The integral itself is discretized and solved using the Gauss–Legendre integration method. A matrix equation is formed by choosing collocation points midway between the Gauss nodes plus one point at the leading edge of the opening. The Kutta condition is imposed at the leading edge of the test section which dictates that $\bar{\xi}_r = 0$ on the leading edge collocation point and on the next nearest collocation point. Having $\bar{\xi}_r$ specified on two collocation points allows $\bar{\alpha}_{1,2}$ to be inserted into the list of unknowns in place of the two known $\bar{\xi}_r$ values. Once $\bar{\xi}_r$ is known along the length of the test section, the Rayleigh conductivity is calculated by numerical integration, i.e.,

$$K_R = \frac{\mathrm{i}\omega \rho_\infty Q(\omega)}{p_i} = 2\pi\alpha\beta \int_{-\bar{Z}}^{\bar{Z}} \bar{\xi}_r(\bar{z})\, \mathrm{d}\bar{z} = 2\pi a \beta \sum_{j=3}^{N} \bar{\xi}_{r_j} \mathrm{d}\bar{z}_j. \tag{28}$$

3. RESULTS

3.1. FORCED MOTION

The results of the solution to equations (27) and (28) are described in this section. Typically, the real and negative imaginary parts of the Rayleigh conductivity are plotted as a function of the Strouhal number (i.e., Γ versus $\bar{\sigma}$ and Δ versus $\bar{\sigma}$, where $K_r/2a = \Gamma - \mathrm{i}\Delta$). Here, the Rayleigh conductivity has been non-dimensionalized by $2a$. Preliminary results for the conductivity of the forced problem presented in

reference [5] have been corrected for an implementation error. The main conclusions from the preliminary study remain unchanged.

Figure 2 shows the conductivity for a fixed length-to-diameter ratio of 1·0 and increasing Mach numbers from 0·001 to 0·5. Several discretization schemes for solving the integral equation (27) were tested. All gave the same result, but the Gauss–Legendre method needed the smallest grid and took the shortest time. Using this method, each Mach number case shown in Figure 2 takes approximately 3 CPU min to calculate.

In Figure 2, the negative imaginary part of the Rayleigh conductivity is shown as the solid line. The imaginary part of the Rayleigh conductivity identifies the frequency regimes in which the vortex sheet motion will be negatively damped. When the imaginary part of the conductivity is positive, i.e., Δ is negative, the vortex sheet will absorb energy from the applied load and use this energy to sustain

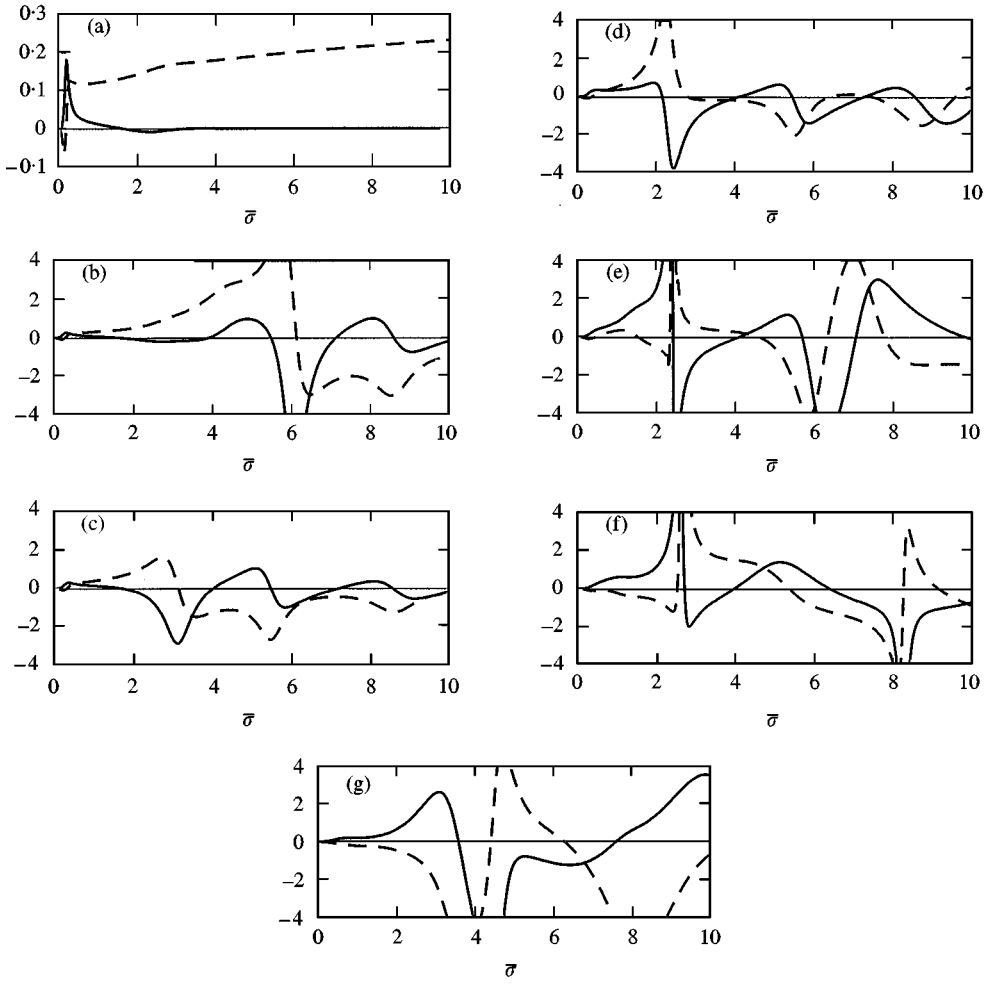

Figure 2. $K_R/2a$: real part (– – –), negative imaginary part (—): (a) $M = 0{\cdot}001$, (b) $M = 0{\cdot}05$, (c) $M = 0{\cdot}1$, (d) $M = 0{\cdot}2$, (e) $M = 0{\cdot}3$, (f) $M = 0{\cdot}4$, (g) $M = 0{\cdot}5$.

the growth of the motion of the sheet which subsequently creates tonal noise. Figure 2(a) shows that, in the incompressible limit, the Rayleigh conductivity for the cylindrical duct configuration is similar to the Rayleigh conductivity for one-sided incompressible grazing flow past a wall aperture [4]. One can also see in Figure 2, that for Mach numbers less than 0·2, the Strouhal number bands in which the imaginary part is positive (solid line dips below the x-axis) remain approximately the same: (2·0, 4·0), (5·7, 7·0), and (8·6, 10·4). The Strouhal number is the ratio of the radial frequency to the fluid flow speed in the duct; therefore, the fact that the Strouhal number bands stay the same as M increases implies that the frequencies at which the forced vortex sheet motion creates tonal noise increase proportionally to the Mach number.

As the Mach number increases past the incompressible regime ($M < 0{\cdot}3$) into the compressible regime ($M \geqslant 0{\cdot}3$), the Strouhal number bands where Δ drops below the real axis shift to higher Strouhal numbers, with the highest bands shifting the most. Thus, for higher flow speeds in the duct, the possible forced frequencies increase non-linearly with Mach number.

The plots in Figure 3 show the effect of the duct gap length-to-diameter ratio on the Rayleigh conductivity. At a fixed Mach number of 0·2, the Rayleigh

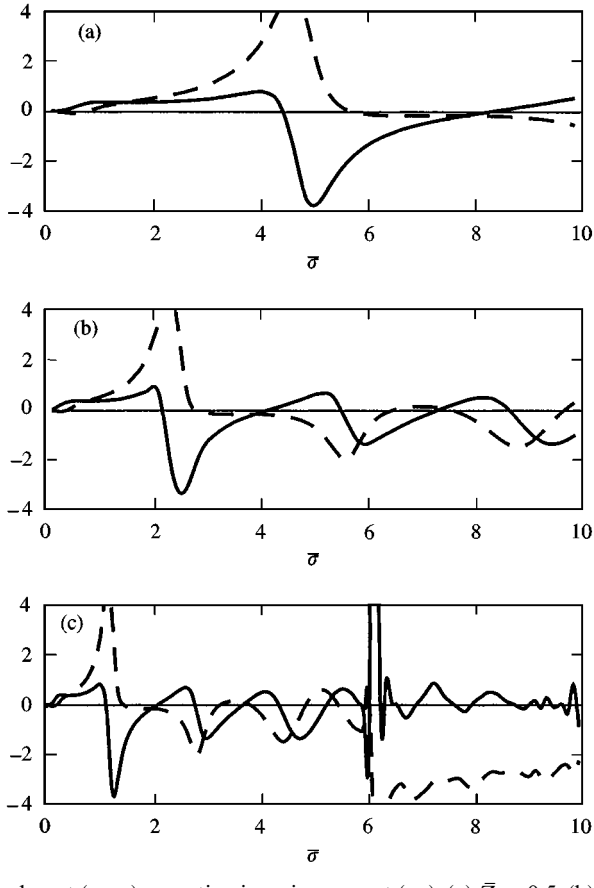

Figure 3. $K_R/2a$: real part (– – –), negative imaginary part (—): (a) $\bar{Z} = 0{\cdot}5$, (b) $\bar{Z} = 1{\cdot}0$, (c) $\bar{Z} = 2{\cdot}0$.

conductivity was calculated for duct gap length-to-diameter ratios of 0·5, 1·0, and 2·0. As the length-to-diameter ratio increases, the first Strouhal number regimes where K_R has a positive imaginary part become centered on smaller Strouhal numbers and the total number of such regimes located between 0 and 10 increases. Lower frequency applied loads lead to lower wavenumber variation of the vortex sheet displacement along the gap. Thus, the gap length must be long, for the low-frequency forcing to produce a three-way coupling between the initial shedding, secondary shedding due to the acoustic pulse from the downstream edge, and the applied load, that will amplify the motion of the vortex sheet. Whereas when the gap length is shorter, coupling that will enhance the vortex sheet motion can occur only at higher frequency (i.e., shorter wavelength of vortex motion displacement along the gap).

3.2. RESONANCE

The Rayleigh conductivity parameter can also be used to determine the frequencies at which the vortex sheet motion will resonate. From equation (1) it is clear that the poles of the conductivity signify frequencies at which the rate of volume flux will be non-zero and thus physically these frequencies represent the possible self-oscillation frequencies of the system (i.e., the frequencies at which the shear layer will continue to oscillate once the forcing is terminated). When the imaginary part of the pole is in the upper half of the complex plane, the system is unstable and the vortex sheet motion will grow in the absence of an external force. Physically, the real part of the unstable poles represent the frequencies at which the shear layer spanning from the inlet to the exit may produce tones [2]. For self-oscillation, the initial vortex shedding occurs because of unsteady disturbances in the wall boundary layer upstream of the inlet edge.

For Mach numbers 0·05, 0·1, 0·2, and 0·5, the quantity $|1/K_R(\bar{\sigma})|$, has been plotted over a set of complex reduced frequencies with real and imaginary parts ranging from 0 to 10 (see Figure 4). The poles of the conductivity coincide with the Strouhal numbers for which $|1/K_R(\bar{\sigma}_p)| = 0$. For each Mach number, there are many dark regions which indicate possible poles. One set of dark regions lies close to the real axis and another set consists of roots with larger imaginary parts. A Newton–Raphson root-finding technique has been employed to calculate the poles exactly. Figure 5 shows the poles which are close to the real axis for varying Mach number and Figure 6 shows the stages of the more unstable poles. Each individual curve indicates an operating stage. The numerical values of the poles for the four lower stages and the three upper stages are given in Tables 1 and 2.

The motion of the shear layer will be self-sustained at the frequencies which correspond to the indicated Strouhal numbers. The pole trajectories cannot be compared to previous analytical studies as was the case for the forced problem. In previous studies, the system was assumed to be incompressible, the normalizing velocity for the Strouhal number was always constant, and the focus was on the difference between having flow on both sides of the wall versus one-sided flow.

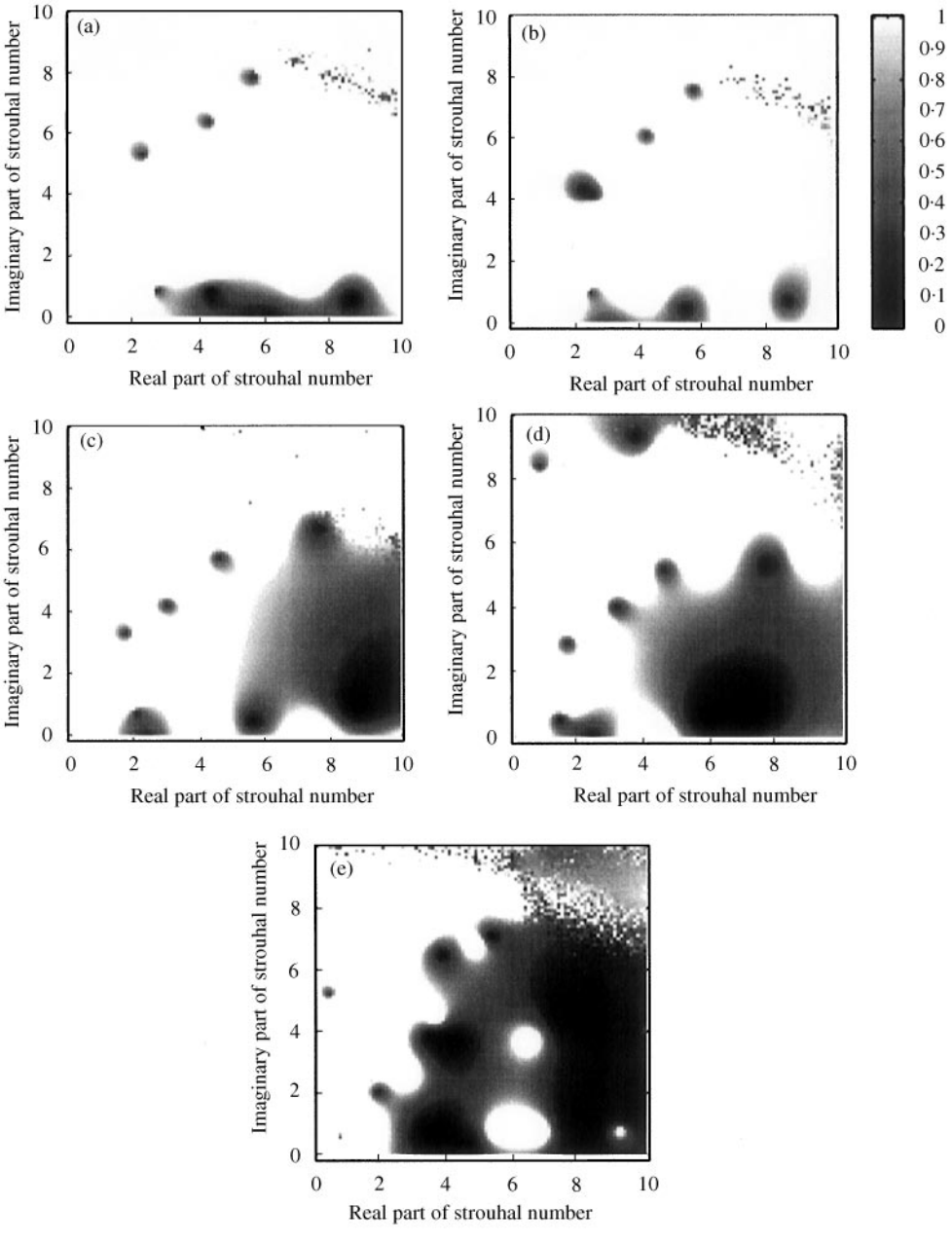

Figure 4. $1/|K_R(\bar{\sigma})|$: $\bar{Z} = 1{\cdot}0$. (a) $M = 0{\cdot}05$, (b) $M = 0{\cdot}1$, (c) $M = 0{\cdot}2$, (d) $M = 0{\cdot}3$, (e) $M = 0{\cdot}5$.

Here, there is flow inside the duct only, i.e., on one side of the wall, and the focus of the study is on the effect of increasing the flow speed.

Paterson *et al.* [1] included a figure of the background noise sound pressure level in the UTRC open-jet wind tunnel. The figure is reproduced in Figure 7. The inlet nozzle was a 31 in × 21 in rectangle with 5 in radius rounded corners. The test

TABLE 1

Poles of the Rayleigh conductivity closest to the real axis

	Real and imaginary parts of $\bar{\sigma}$							
Mach	Stage 1		2		3		4	
0·05	2·72,	0·81	4·30,	0·74	6·03,	− 0·33	8·58,	0·58
0·06	2·72,	0·83	4·17,	0·27	5·53	− 0·08	8·60,	0·64
0·07	2·70,	0·87	3·83,	− 0·11	5·43,	0·21	8·62,	0·66
0·08	2·66,	0·89	3·52,	− 0·29	5·44,	0·33	8·63,	0·66
0·09	2·62,	0·90	3·27,	− 0·38	5·46,	0·38	8·64,	0·66
0·10	2·57,	0·91	3·08,	− 0·42	5·48,	0·41	8·64,	0·66
0·11	2·52,	0·90	2·93,	− 0·43	5·49,	0·42	8·65,	0·66
0·12	2·46,	0·89	2·81,	− 0·43	5·50,	0·42	8·66,	0·66
0·13	2·41,	0·88	2·71,	− 0·42	5·51,	0·42	8·66,	0·67
0·14	2·36,	0·86	2·62,	− 0·41	5·52,	0·42	8·67,	0·68
0·15	2·31,	0·83	2·55,	− 0·38	5·53,	0·42	8·68,	0·69
0·16	2·26,	0·81	2·49,	− 0·36	5·53,	0·42	8·69,	0·71
0·17	2·21,	0·78	2·44,	− 0·33	5·54,	0·41	8·70,	0·73
0·18	2·16,	0·75	2·40,	− 0·29	5·55,	0·41	8·71,	0·77
0·19	2·11,	0·72	2·37,	− 0·26	5·56,	0·41	8·72,	0·82
0·20	2·05,	0·68	2·34,	− 0·22	5·57,	0·41	8·73,	0·90
0·21	2·00,	0·65	2·32,	− 0·19	5·59,	0·40	8·71,	1·01
0·22	1·94,	0·62	2·32,	− 0·15	5·60,	0·40	8·64,	1·14
0·23	1·87,	0·58	2·32,	− 0·12	5·62,	0·40	8·50,	1·25
0·24	1·80,	0·56	2·32,	− 0·09	5·64,	0·41	8·33,	1·30
0·25	1·73,	0·54	2·34,	− 0·06	5·67,	0·41	8·14,	1·31
0·26	1·66,	0·52	2·35,	− 0·05	5·70,	0·41	7·96,	1·28
0·27	1·59,	0·51	2·37,	− 0·03	5·74,	0·42	7·78,	1·21
0·28	1·53,	0·50	2·39,	− 0·03	5·79,	0·44	7·60,	1·11
0·29	1·47,	0·50	2·41,	− 0·02	5·86,	0·47	7·41,	0·97
0·30	1·41,	0·49	2·42,	− 0·02	5·95,	0·53	7·21,	0·75
0·31	1·35,	0·49	2·44,	− 0·02	6·05,	0·70	7·02,	0·37
0·32	1·30,	0·49	2·46,	− 0·02	5·99,	0·91	6·99,	− 0·22
0·33	1·25,	0·49	2·48,	− 0·02	5·88,	1·04	6·65,	− 0·77
0·34	1·20,	0·49	2·50,	− 0·03	5·76,	1·11	6·29,	− 0·99
0·35	1·16,	0·49	2·52,	− 0·03	5·65,	1·16	5·99,	− 1·11
0·36	1·11,	0·49	2·54,	− 0·04	5·54,	1·18	5·73,	− 1·17
0·37	1·07,	0·49	2·56,	− 0·05	5·43,	1·19	5·50,	− 1·19
0·38	1·03,	0·49	2·58,	− 0·06	5·33,	1·19	5·29,	− 1·19
0·39	0·99,	0·49	2·61,	− 0·07	5·24,	1·18	5·09,	− 1·17
0·40	0·95,	0·49	2·64,	− 0·09	5·14,	1·16	4·90,	− 1·13
0·41	0·92,	0·49	2·67,	− 0·11	5·05,	1·13	4·73,	− 1·08
0·42	0·88,	0·49	2·71,	− 0·13	4·96,	1·09	4·56,	− 1·01
0·43	0·85,	0·49	2·76,	− 0·16	4·86,	1·05	4·39,	− 0·93
0·44	0·82,	0·49	2·83,	− 0·21	4·77,	0·99	4·21,	− 0·82
0·45	0·79,	0·49	2·91,	− 0·28	4·68,	0·92	4·03,	− 0·68
0·46	0·76,	0·49	3·01,	− 0·42	4·59,	0·83	3·83,	− 0·45
0·47	0·73,	0·48	2·98,	− 0·66	4·50,	0·71	3·73,	− 0·08
0·48	0·70,	0·48	2·86,	− 0·81	4·45,	0·54	3·71,	0·26
0·49	0·68,	0·48	2·74,	− 0·90	4·50,	0·40	3·60,	0·51
0·50	0·65,	0·47	2·62,	− 0·96	4·56,	0·33	3·48,	0·65

TABLE 1

Continued

	Real and imaginary parts of $\bar{\sigma}$							
Mach	Stage 1		2		3		4	
0·51	0·63,	0·47	2·51,	− 1·00	4·61,	0·29	3·38,	0·75
0·52	0·60,	0·46	2·41,	− 1·02	4·63,	0·27	3·28,	0·81
0·53	0·58,	0·46	2·32,	− 1·03	4·65,	0·26	3·20,	0·86
0·54	0·56,	0·46	2·23,	− 1·04	4·67,	0·25	3·12,	0·89
0·55	0·53,	0·45	2·14,	− 1·03	4·67,	0·25	3·05,	0·91
0·56	0·51,	0·44	2·07,	− 1·03	4·66,	0·25	2·98,	0·92
0·57	0·49,	0·44	1·99,	− 1·01	4·64,	0·24	2·91,	0·93
0·58	0·47,	0·43	1·93,	− 1·00	4·61,	0·24	2·84,	0·92
0·59	0·45,	0·43	1·86,	− 0·98	4·54,	0·23	2·77,	0·91
0·60	0·43,	0·42	1·80,	− 0·96	4·44,	0·22	2·70,	0·89
0·61	0·42,	0·41	1·75,	− 0·94	4·32,	0·22	2·64,	0·87
0·62	0·40,	0·41	1·69,	− 0·92	4·18,	0·23	2·57,	0·85
0·63	0·38,	0·40	1·64,	− 0·90	4·03,	0·24	2·50,	0·83
0·64	0·36,	0·39	1·59,	− 0·87	3·88,	0·25	2·43,	0·80
0·65	0·35,	0·39	1·55,	− 0·85	3·74,	0·25	2·36,	0·77
0·66	0·33,	0·38	1·50,	− 0·83	3·60,	0·26	2·28,	0·75
0·67	0·31,	0·37	1·46,	− 0·80	3·46,	0·26	2·21,	0·72
0·68	0·30,	0·36	1·42,	− 0·78	3·33,	0·26	2·15,	0·69
0·69	0·28,	0·35	1·38,	− 0·75	3·21,	0·26	2·08,	0·66
0·70	0·27,	0·35	1·34,	− 0·73	3·09,	0·26	2·01,	0·63
0·71	0·26,	0·34	1·30,	− 0·70	2·97,	0·26	1·95,	0·61
0·72	0·24,	0·33	1·27,	− 0·68	2·86,	0·26	1·88,	0·58
0·73	0·23,	0·32	1·23,	− 0·65	2·75,	0·25	1·82,	0·55
0·74	0·21,	0·31	1·20,	− 0·63	2·64,	0·25	1·76,	0·52
0·75	0·20,	0·30	1·16,	− 0·60	2·54,	0·24	1·70,	0·50
0·76	0·19,	0·29	1·13,	− 0·58	2·43,	0·23	1·65,	0·47
0·77	0·17,	0·29	1·10,	− 0·55	2·33,	0·23	1·59,	0·44
0·78	0·16,	0·28	1·06,	− 0·53	2·23,	0·22	1·54,	0·41
0·79	0·15,	0·27	1·03,	− 0·50	2·13,	0·21	1·49,	0·38
0·80	0·14,	0·26	1·00,	− 0·47	2·03,	0·21	1·44,	0·35

section was 22·5 in long and was only semi-open in that it had plates along two sides. The collector was also a rounded rectangle just slightly larger than the inlet nozzle. The SPL spectrum for a flow speed of 575 ft/s contained several spikes. The tones were later eliminated by redesigning the inlet using tabs. However, the spectrum without the tabs can be used to validate the results shown in Figures 5 and 6 for the resonant frequencies of the system. The duct in the experiment is a rounded rectangle that is approximated here as a cylinder. The diagonal of the rectangle is 37 in. If this is used as the diameter of the model cylindrical duct then the length-to-diameter ratio in the model is approximately 1·6. If however a cylinder that can be completly inscribed in the rectangle is used, the diameter would be 21 in with a corresponding and the length-to-diameter ratio of approximately 1·0.

TABLE 2

Poles of the Rayleigh conductivity farther above from the real axis

	Real and imaginary parts of $\bar{\sigma}$					
Mach	Stage 1		2		3	
0·05	2·21,	5·24	3·21,	3·88	4·27,	6·34
0·06	2·20,	5·04	3·13,	3·89	4·25,	6·27
0·07	2·20,	4·85	2·98,	3·91	4·26,	6·20
0·08	2·22,	4·67	2·84,	3·94	4·27,	6·14
0·09	2·25,	4·47	2·71,	4·00	4·29,	6·09
0·10	2·28,	4·20	2·61,	4·14	4·31,	6·05
0·11	2·14,	3·97	2·68,	4·26	4·34,	6·01
0·12	2·04,	3·84	2·74,	4·29	4·36,	5·98
0·13	1·96,	3·74	2·79,	4·29	4·39,	5·94
0·14	1·89,	3·65	2·82,	4·28	4·42,	5·91
0·15	1·84,	3·57	2·85,	4·27	4·44,	5·88
0·16	1·80,	3·50	2·88,	4·26	4·47,	5·85
0·17	1·77,	3·44	2·90,	4·24	4·50,	5·82
0·18	1·74,	3·38	2·93,	4·23	4·52,	5·79
0·19	1·72,	3·33	2·94,	4·20	4·55,	5·76
0·20	1·70,	3·28	2·97,	4·19	4·57,	5·73
0·21	1·68,	3·23	2·99,	4·17	4·59,	5·69
0·22	1·67,	3·18	3·01,	4·15	4·62,	5·65
0·23	1·66,	3·14	3·03,	4·14	4·63,	5·60
0·24	1·66,	3·10	3·05,	4·12	4·65,	5·55
0·25	1·66,	3·06	3·07,	4·10	4·66,	5·49
0·26	1·65,	3·02	3·09,	4·08	4·66,	5·43
0·27	1·66,	2·98	3·11,	4·06	4·66,	5·37
0·28	1·66,	2·94	3·13,	4·04	4·66,	5·30
0·29	1·66,	2·90	3·15,	4·03	4·65,	5·23
0·30	1·67,	2·86	3·17,	4·01	4·63,	5·16
0·31	1·68,	2·83	3·19,	3·99	4·61,	5·09
0·32	1·69,	2·79	3·22,	3·97	4·59,	5·02
0·33	1·70,	2·76	3·24,	3·96	4·56,	4·95
0·34	1·71,	2·72	3·26,	3·94	4·52,	4·87
0·35	1·72,	2·68	3·28,	3·92	4·49,	4·80
0·36	1·74,	2·65	3·31,	3·91	4·45,	4·73
0·37	1·75,	2·61	3·34,	3·90	4·40,	4·65
0·38	1·77,	2·57	3·36,	3·88	4·36,	4·58
0·39	1·78,	2·53	3·39,	3·87	4·31,	4·51
0·40	1·80,	2·49	3·43,	3·86	4·26,	4·44
0·41	1·81,	2·45	3·46,	3·85	4·22,	4·37
0·42	1·83,	2·41	3·50,	3·85	4·17,	4·30
0·43	1·84,	2·36	3·53,	3·84	4·12,	4·23
0·44	1·86,	2·32	3·57,	3·84	4·07,	4·15
0·45	1·87,	2·27	3·60,	3·85	4·04,	4·07
0·46	1·88,	2·22	3·62,	3·87	4·02,	3·97
0·47	1·89,	2·17	3·62,	3·89	4·03,	3·87
0·48	1·89,	2·12	3·58,	3·89	4·07,	3·80
0·49	1·90,	2·07	3·54,	3·88	4·13,	3·74
0·50	1·90,	2·01	3·50,	3·84	4·19,	3·68

TABLE 2

Continued

	Real and imaginary parts of $\bar{\sigma}$					
Mach	Stage 1		2		3	
0·51	1·90,	1·96	3·46,	3·80	4·25,	3·64
0·52	1·89,	1·91	3·42,	3·76	4·32,	3·60
0·53	1·88,	1·86	3·38,	3·70	4·40,	3·55
0·54	1·87,	1·81	3·34,	3·65	4·48,	3·50
0·55	1·85,	1·76	3·30,	3·59	4·57,	3·44
0·56	1·84,	1·71	3·27,	3·53	4·67,	3·35
0·57	1·82,	1·67	3·23,	3·46	4·75,	3·23
0·58	1·80,	1·63	3·20,	3·39	4·78,	3·05
0·59	1·77,	1·59	3·17,	3·32	4·73,	2·88
0·60	1·75,	1·55	3·15,	3·24	4·62,	2·76
0·61	1·72,	1·52	3·12,	3·16	4·50,	2·68
0·62	1·69,	1·49	3·10,	3·07	4·38,	2·63
0·63	1·66,	1·46	3·08,	2·98	4·27,	2·60
0·64	1·64,	1·43	3·05,	2·88	4·16,	2·59
0·65	1·61,	1·40	3·01,	2·77	4·08,	2·59
0·66	1·58,	1·38	2·97,	2·66	4·01,	2·60
0·67	1·54,	1·36	2·92,	2·56	3·96,	2·60
0·68	1·51,	1·34	2·86,	2·46	3·92,	2·60
0·69	1·48,	1·32	2·79,	2·36	3·90,	2·59
0·70	1·44,	1·31	2·72,	2·28	3·88,	2·56
0·71	1·41,	1·29	2·65,	2·20	3·87,	2·53
0·72	1·37,	1·27	2·59,	2·13	3·87,	2·49
0·73	1·33,	1·26	2·52,	2·06	3·88,	2·45
0·74	1·30,	1·24	2·46,	1·99	3·91,	2·38
0·75	1·26,	1·23	2·40,	1·93	3·93,	2·26
0·76	1·21,	1·21	2·34,	1·86	3·91,	2·11
0·77	1·17,	1·19	2·29,	1·80	3·84,	1·98
0·78	1·13,	1·18	2·23,	1·74	3·73,	1·86
0·79	1·08,	1·16	2·18,	1·67	3·59,	1·75
0·80	1·03,	1·14	2·12,	1·61	3·41,	1·67

The flow speed translates to a Mach number of 0·52 when calculated using the speed of sound as 1115 ft/s. The real part of the Strouhal numbers for the unstable poles for a cylindrical duct with gap length-to-diameter ratio of 1·0 and a flow speed Mach number of 0·52 can be found from either Figures 5 and 6 or Tables 1 and 2. The values from the lower stages are 0·601, 3·28, and 4·63; the values from the upper stages are 1·89, 3·42, 4·32. The frequency corresponding to these Strouhal numbers is calculated easily using

$$f = \frac{\omega}{2\pi} = \frac{\bar{\sigma} U}{2\pi a},$$

where a is roughly 10·5 in, and thus the predicted frequencies are 63, 343, and 484 Hz for the lower stages and 198, 358 and 452 Hz for the upper stages. These

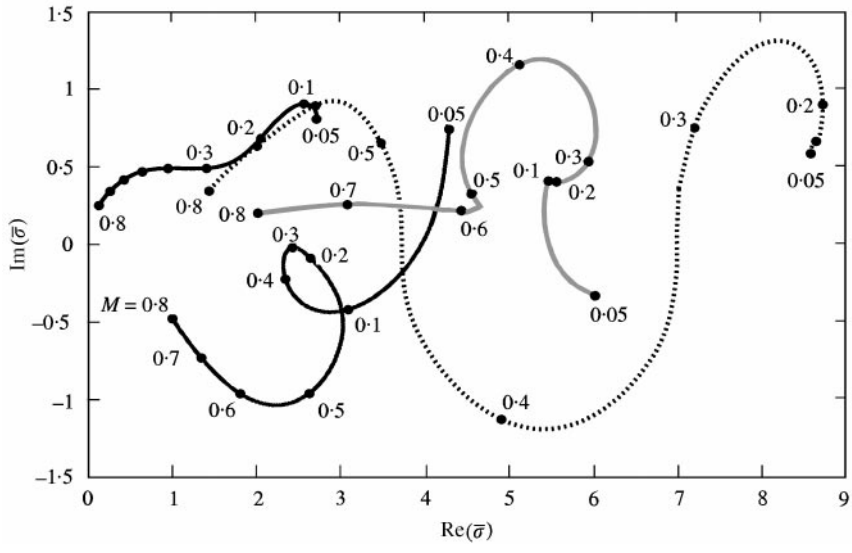

Figure 5. Set of poles of the Rayleigh conductivity close to the real axis for varying Mach number.

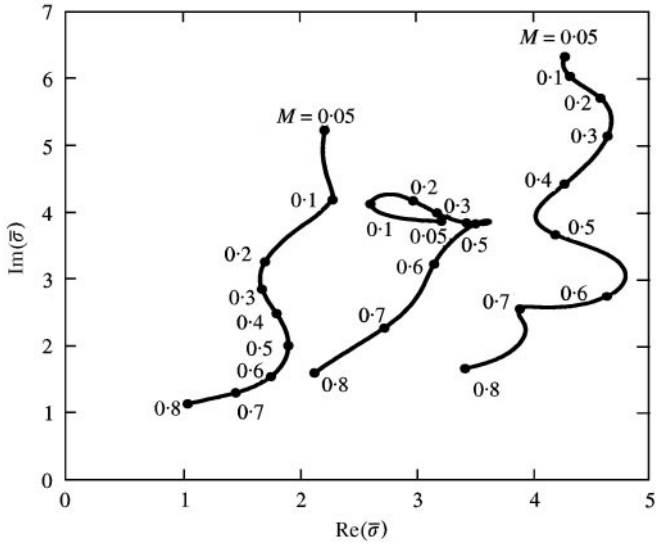

Figure 6. Set of poles of the Rayleigh conductivity farther from the real axis for varying Mach number.

frequencies are upper estimates on the true frequencies, because the equivalent length-to-diameter, $\bar{Z}$, used in the model is the lower bound of the possible choices for the ratio. Figure 3 shows that the dependence on $\bar{Z}$ of the Strouhal number is of the form $1/\bar{Z}$, so that when $\bar{Z}$ is 1·6, the frequencies become 39, 214, and 322 Hz for the lower stages and 132, 239, and 302 Hz for the upper stages. The 1/3 octave band frequencies reported by Paterson *et al.* [1] were centered at 50, 200, and 400 Hz. (Figure 7 also shows a tone centered at 800 Hz which is outside of the range of

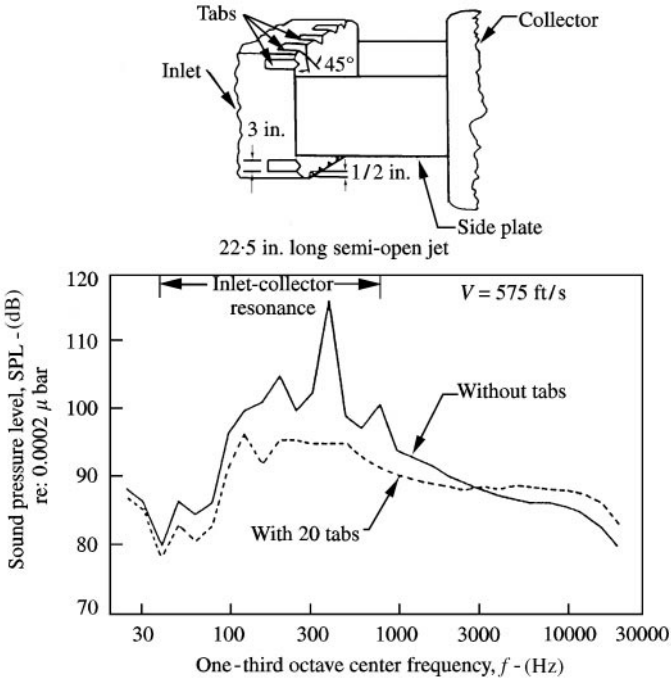

Figure 7. Background sound pressure level measurements from UTRC acoustic research tunnel [1, p. 430].

frequencies computed in this study.) Therefore, the measured frequencies lie in the bands: (45–56 Hz), (180–224 Hz), (355–450 Hz).

The dotted line in the experimental results is the sound pressure level after the inlet was redesigned to have tabs. In the redesigned tunnel, the lowest tone still exists and the upper tones are eradicated; however, another tone appears. This tone may exist when there are no tabs on the inlet, but its magnitude does not allow it to stand out from the background noise at that frequency. The frequency for this secondary tone is in the 1/3 octave band centered at 125 Hz in the experiments. This tone coincides with the predicted frequency from the first upper stage. This is the only predicted frequency in the upper stage that does not have a lower stage frequency close to it and thus it is not surprising that it is less dominant than the other tones. Overall, the agreement between the predicted resonant frequencies and those reported in the experiment is excellent even though the model geometry does not match the experimental configuration perfectly.

4. CONCLUSIONS

A method has been presented for approximating the frequencies which correspond to resonant and forced shear layer motion in the outer edge of a thin-walled cylindrical duct with a gap. These frequencies are of interest because of their association with tonal noise production by the system. This paper corrects the preliminary results presented in reference [5] for the forced response and extends the study to include predictions of the resonant frequencies.

The method is based on the linearized equations of motion and relies on the analysis of the Rayleigh conductivity parameter. Because the method is based on linear theory, only the frequency and not the amplitude of the self-sustaining oscillation of the shear layer can be calculated.

For the forced problem, the frequency regimes in which the shear layer motion will amplify when an external load is applied are related to the Strouhal number regimes for which the imaginary part of the Rayleigh conductivity is positive. At low Mach numbers, the frequency bands for which forced shear layer motion amplification will occur in the cylindrical duct gap compare well with those found in similar studies involving incompressible flow past wall openings. Further, it is shown that the center frequencies of the regimes increase as the Mach number increases but decrease as the gap length-to-diameter ratio increases.

The real part of the poles of the Rayleigh conductivity correspond to the possible self-oscillation Strouhal numbers, with resonance occurring when the imaginary part of the Strouhal number is positive (i.e., $\mathrm{Im}(\bar{\sigma}) > 0$). The predicted resonant frequencies are obtained from the Strouhal number which is based on the radius of the test section and the velocity of the mean flow. The poles are found for Mach numbers ranging from 0·001 to 0·8. Two dominant sets of frequency stages are found for flow through a cylindrical duct with a gap. One set of stages has Strouhal numbers with imaginary parts close to the real axis while the other set has larger positive imaginary parts. Good comparison between the predicted resonant frequencies and experimental data at a Mach number of 0·52 helps to validate the method.

The Green's function required for the calculation of the conductivity is easily obtained for the cylindrical duct, and its behavior is captured with an asymptotic form. This adds to the speed of the computation. For other duct shapes, the results for the cylindrical duct may approximate the resonant frequencies well as shown in the experimental validation. However, one can calculate the true frequencies for different duct shapes by redefining Green's function. For many duct shapes the Green's function will have to be calculated numerically which will slow the computation. Overall, the method of analysis has been shown to work well, and when compressibility effects are added, the method still maintains its main advantage over other methods by providing predictions quickly.

ACKNOWLEDGMENTS

The author would like to thank Professors Michael Howe and Luigi Morino for their helpful comments with regard to this work. Also, Professor Paul Barbone is acknowledged for his willingness to discuss Green's function derivation.

REFERENCES

1. R. W. Paterson, P. G. Vogt and W. M. Foley 1973 *Journal of Aircraft* **10**, 427–433. Design and development of the United Aircraft Research Laboratories Acoustic Research Tunnel.

2. M. S. Howe 1997 *Journal of Fluid Mechanics* **330**, 61–84. Edge, cavity and aperture tones at very low Mach numbers.
3. M. S. Howe, M. I. Scott and S. R. Sipcic 1996 *Proceedings of the Royal Society of London A* **452**, 2303–2317. The influence of tangential mean flow on the Rayleigh conductivity of an aperture.
4. S. M. Grace, K. P. Horan and M. S. Howe 1998 *Journal of Fluid and Structures* **12**, 335–351. The influence of shape on the Rayleigh conductivity of a wall aperture in the presence of grazing flow.
5. S. M. Grace 1998 *Proceedings of the 4th AIAA/CEAS Aeroacoustics Conference*, *AIAA Paper No.* 98–2304. Acoustic energy absorption by a shear layer.
6. M. S. Howe 1997 *Journal of the Acoustical Society of America* **102**, 772–780. Low Strouhal number instabilities of flow over apertures and wall cavities.
7. S. M. Grace, T. H. Wood and M. S. Howe 1999 *Proceedings of the Royal Society of London* **455**, 2055–2066. Stability of high Reynolds number flow past a circular aperture.
8. M. S. Howe 1981 *Philosophical Transactions of the Royal Society of London* A **303**, 151–180. On the theory of unsteady shearing flow over a slot.
9. M. Abromowitz and I. A. Stegun 1965 *Handbook of Mathematical Tables.* (Eq. 9.1.8). New York: Dover Publications Inc.
10. H. Batemean 1954 *Tables of Integral Transforms* (Eqs. 1.38, 1.39) New York, McGraw-Hill.

APPENDIX A: ASYMPTOTIC FORM OF GREEN'S FUNCTION

The Green's functions for the interior and exterior of the cylinder are respectively

$$G_i = \frac{1}{2\pi}\int_{-\infty}^{\infty} \frac{I_0(\sqrt{k^2 - K_i^2}\,\tilde{r})\,\mathrm{e}^{\mathrm{i}k(z_0 - z)}\,\mathrm{d}k}{\tilde{a}\sqrt{k^2 - K_i^2}\,I_1(\sqrt{k^2 - K_i^2}\,\tilde{a})}, \tag{A.1}$$

$$G_o = \frac{1}{2\pi}\int_{-\infty}^{\infty} \frac{-\mathscr{K}_0(\sqrt{k^2 - K_o^2}\,r)\,\mathrm{e}^{\mathrm{i}k(z_0 - z)}\,\mathrm{d}k}{a\sqrt{k^2 - K_o^2}\,\mathscr{K}_1(\sqrt{k^2 - K_o^2}\,a)}. \tag{A.2}$$

In this application $r \to a$ and we are interested in the case when z_0 is close to z. Under these conditions the integral can be simplified by substituting into the integrals the quantity

$$\lambda = k(z_0 - z), \quad \mathrm{d}\lambda = \mathrm{d}k(z_0 - z),$$

which gives for the inner Green's function

$$G_i = \lim_{(z_0 - z)\to 0} \frac{1}{2\pi}\int_{-\infty}^{\infty} \frac{I_0\left(\sqrt{\dfrac{\lambda^2}{(z_0 - z)^2} - K_i^2}\,\tilde{a}\right)\mathrm{e}^{\mathrm{i}\lambda}}{\sqrt{\lambda^2 - (z_0 - z)^2 K_i^2}\,I_1(\sqrt{\lambda^2/(z_0 - z)^2 - K^2}\,\tilde{a})}\,\mathrm{d}\lambda.$$

One can then use the asymptotic behavior of the Bessel functions:

$$\lim_{x\to\infty}\frac{I_0(x)}{I_1(x)} \sim 1, \quad \lim_{x\to\infty}\frac{\mathscr{K}_0(x)}{\mathscr{K}_1(x)} \sim 1,$$

to obtain a limiting form of the integral

$$G_i \sim \lim_{(z_0 - z) \to 0} \frac{1}{2\pi} \int_{-\infty}^{\infty} \frac{e^{i\lambda}}{\sqrt{\lambda^2 - (z_0 - z)^z K_i^2}} d\lambda = \lim_{(z_0 - z) \to 0} \frac{1}{\pi} \int_0^{\infty} \frac{\cos(\lambda)}{\sqrt{\lambda^2 - (z_0 - z)^z K_i^2}} d\lambda$$

$$= - \lim_{(z_0 - z) \to 0} \frac{i}{2} H_0^2(K_i | z_0 - z|)$$

$$\sim - \frac{1}{\pi} \ln(K_i | z_0 - z|),$$

where $H_0^{(2)} = J_0 - iY_0$ [9]. A similar simplification follows for the outer Green's function.